JGR Atmospheres

RESEARCH ARTICLE
10.1029/2025JD044677

Special Collection:
Biomass Burning Uncertainties: Emissions, Chemistry, and Physics

Comparisons of High Spatiotemporal Resolution Air Quality Modeling Frameworks for Prescribed Burning Simulations at a Military Base in the Southeastern United States

Zongrun Li[1], Rime El Asmar[2], Susan O'Neill[3], Yongtao Hu[1], Haofei Yu[4], Yunyao Li[5], David J. Tanner[2], L. Gregory Huey[2], Rodney J. Weber[2], Armistead G. Russell[1], and M. Talat Odman[1]

[1]School of Civil and Environmental Engineering, Georgia Institute of Technology, Atlanta, GA, USA, [2]School of Earth and Atmospheric Sciences, Georgia Institute of Technology, Atlanta, GA, USA, [3]United States Department of Agriculture Forest Service, Pacific Northwest Research Station, Seattle, WA, USA, [4]Department of Civil, Environmental, and Construction Engineering, University of Central Florida, Orlando, FL, USA, [5]Earth and Environmental Sciences, The University of Texas at Arlington, Arlington, TX, USA

Abstract High spatiotemporal resolution air quality modeling is essential for air quality impact assessments and decision-making for prescribed burns. Accurate representation of the heterogeneous distribution of fuels and the structure of smoke plumes requires high-resolution modeling frameworks. In this study, we conducted simulations of prescribed burns in Fort Benning, Georgia, with BlueSky-CMAQ and WRF-SFIRE modeling frameworks and compared the differences between the results. BlueSky-CMAQ was run at a 1-km resolution, while WRF-SFIRE operated at a 200-m resolution, both generating outputs every 20 min. We compared the emission profiles, smoke plume structures, and ground-level concentrations of pollutants between these two modeling frameworks. We used measurements of winds and pollutant concentrations collected at the military base to evaluate model performance and identify critical factors affecting simulation accuracy, including the plume rise scheme, uncertainties from satellite-detected fire start time and FRP, and biases in wind simulations. All settings of the simulation frameworks showed a correlation higher than 0.21 with measurements of $PM_{2.5}$ during the prescribed burning periods. The WRF-SFIRE had the highest correlation ($r = 0.29$) with observation, and the BlueSky-CMAQ with Freitas plume rise scheme showed the best performance for simulating the intensity of detected smoke, with a regression slope of 0.93. The findings and lessons learned are presented to inform future field measurement design and model implementations for studying the prescribed fire impacts on local air quality.

Plain Language Summary Smoke modeling is critical for air quality assessments and prescribed burn decisions. The study used two high-resolution models, a fire behavior model, and a chemical transport model, to simulate smoke from prescribed burns at a southeastern US military base. Models were evaluated with observations, and critical factors affecting simulation accuracy were identified. Results showed the fire behavior model performed better, highlighting the importance of plume dynamics in accurate smoke simulations.

Key Points:

- WRF-SFIRE and CMAQ were applied to simulate smoke from prescribed burns; WRF-SFIRE showed higher correlation with observations
- Differences in emissions and plume heights between WRF-SFIRE and CMAQ significantly affected surface smoke concentrations
- Fire start time, variability in FRP across satellites, and wind simulation biases are critical uncertainty sources in smoke modeling

Supporting Information:

Supporting Information may be found in the online version of this article.

Correspondence to:

M. T. Odman,
odman@gatech.edu

Citation:

Li, Z., El Asmar, R., O'Neill, S., Hu, Y., Yu, H., Li, Y., et al. (2025). Comparisons of high spatiotemporal resolution air quality modeling frameworks for prescribed burning simulations at a military base in the southeastern United States. *Journal of Geophysical Research: Atmospheres*, *130*, e2025JD044677. https://doi.org/10.1029/2025JD044677

Received 21 JUN 2025
Accepted 1 NOV 2025

Author Contributions:

Conceptualization: Zongrun Li, M. Talat Odman
Data curation: Rime El Asmar, Haofei Yu, David J. Tanner, L. Gregory Huey, Rodney J. Weber
Formal analysis: Zongrun Li, M. Talat Odman

1. Introduction

The burned area from wildfires in the United States (US) has shown an increasing trend over recent decades, resulting in higher federal suppression costs (Jaffe et al., 2020). Wildfire risks are expected to increase due to the accumulation of fuels from past fire suppression (Marlon et al., 2012) and increasing fuel aridity (Burke et al., 2021), which is anticipated to persist with ongoing global warming (Westerling et al., 2006). Prescribed burning is an effective land management strategy to reduce wildfire risk by decreasing the accumulation of fuels. Prescribed fires are typically low-intensity burns with a short duration conducted under favorable meteorological conditions to control fire spread and minimize smoke impacts. Prescribed burning has other benefits, including local ecosystem protection (Francos & Úbeda, 2021; Policelli et al., 2019) and biodiversity enhancement (Hunter & Robles, 2020). However, like all types of biomass burning, prescribed burning is a source of smoke that degrades air quality. In the southeastern US, prescribed burns contribute 10%–15% to the annual average ambient $PM_{2.5}$ (particulate matter whose aerodynamic diameters are 2.5 μm or smaller) (Afrin & Garcia-Menendez, 2020; Carter et al., 2023), raising concerns about the health impact of $PM_{2.5}$ from prescribed burns on populations (Huang et al., 2019; Maji et al., 2024a, 2024b).

Funding acquisition: L. Gregory Huey, Rodney J. Weber, Armistead G. Russell, M. Talat Odman
Investigation: Susan O'Neill, Yongtao Hu
Methodology: Zongrun Li, M. Talat Odman
Project administration: M. Talat Odman
Resources: Susan O'Neill, Yunyao Li
Software: Zongrun Li, Susan O'Neill, Yongtao Hu, Yunyao Li, M. Talat Odman
Supervision: Armistead G. Russell, M. Talat Odman
Visualization: Zongrun Li
Writing – original draft: Zongrun Li, M. Talat Odman
Writing – review & editing: Zongrun Li, Rime El Asmar, Susan O'Neill, Yongtao Hu, Haofei Yu, Yunyao Li, David J. Tanner, L. Gregory Huey, Rodney J. Weber, Armistead G. Russell, M. Talat Odman

Accurate air quality modeling frameworks are essential for guiding fire managers in reducing air quality impacts from prescribed burns, improving understanding of health effects of prescribed burn-related air pollution and providing forecasts to protect sensitive populations from smoke exposure. Multiple smoke modeling tools are available to evaluate air quality impacts from smoke and provide information for prescribed fire decisions, including trajectory models, dispersion models, empirical models, chemical transport models, and fire behavior models. Trajectory and dispersion models have low computational requirements due to the simplification of physics and do not account for the chemical reactions in smoke. These models can be used to provide real-time decisions. Simple Smoke Screening Tool (SSST) (Mobley, 1976), Hybrid Single-Particle Lagrangian Integrated Trajectory (HYSPLIT) model (Stein et al., 2015), and VSmoke (Lavdas, 1996) are three commonly used web-based management tools that can provide real-time smoke impacts from prescribed burns. SSST is a model that estimates smoke-sensitive areas based on the Lavdas dispersion index (Lavdas, 1986); HYSPLIT is a Lagrangian trajectory model, and VSmoke is a steady-state Gaussian plume dispersion model. Johnson and Garcia-Menendez (2023) applied these tools to simulate the prescribed burning air quality impacts. The smoke predictions from these tools had low spatial correlations with each other, which led to a concern about using these tools for air quality simulation or exposure evaluation. Empirical models typically use statistical or machine learning methods to develop the relationships between fire-related pollutants and other environmental factors such as geographical patterns, meteorological conditions, and satellite retrievals. Lee and Jaffe (2024) identified smoke days using $PM_{2.5}$ observations and Hazard Mapping System (HMS) data. Then, generalized additive models were built with NO_2 satellite retrieval, meteorological conditions, day of the year, and smoke trajectories as predictors and observed ozone as training targets. Similarly, Childs et al. (2022) also identified smoke days and used a machine learning (ML) model to predict fire-related $PM_{2.5}$. The model was developed using fire indicators from HMS, simulated smoke trajectories, aerosol optical depth retrievals, and meteorological and geographical data to predict $PM_{2.5}$. Raffuse et al. (2024) used the random forest machine learning model to improve upon forecasted $PM_{2.5}$ data from dispersion models, creating a data set for health impact analysis. Chemical transport models (CTMs) account for plume height, temporal profile of fire emissions, smoke transport, and chemical reactions, which can also be applied to understanding fire impacts on air quality. The Community Multiscale Air Quality Modeling System (CMAQ) (Byun & Schere, 2006) is a CTM widely used to evaluate countrywide or regional fire-specific air quality impacts (Baker et al., 2016; Maji et al., 2024a, 2024b; Wilkins et al., 2018). Qiu et al. (2024) compared the ML-derived and CTM-simulated smoke $PM_{2.5}$. The study found that the ML-based approach outperformed the CTM in predicting high smoke levels. However, the CTM-based approach demonstrated better prediction performance when the smoke level was moderate. Another category of models for smoke simulation is fire behavior models, which have the highest level of physics complexity for fire simulations among the discussed models. Instead of using parametrized plume rise schemes and empirical time profiles to distribute fire emissions, which are used in CTMs, the fire behavior models simulate the fire propagation process by considering the interactions between fire and the atmosphere. Then, the emission time profile is estimated based on consumed fuel, and the smoke is elevated by buoyancy generated from the fire heat flux during the fire spreading. WRF-SFIRE is a fire behavior model incorporated in an atmospheric dynamics model, the Weather Research and Forecasting (WRF) model, which was applied to simulate wildfires and prescribed burns (Kochanski et al., 2013; Mallia et al., 2020; Mandel et al., 2014). Atmospheric chemistry can also be considered by coupling the fire behavior model with WRF-Chem (Kochanski et al., 2012), which is a CTM coupled with atmospheric dynamics.

Although some previous studies showed reasonable performance when applying smoke models to simulate daily regional impacts from multiple fire sources, the performance of the smoke models for single-prescribed burn simulations under a high spatiotemporal resolution is not well understood. Except for the fire behavior model WRF-SFIRE, which requires high spatial resolution (subgrid scales less than a few hundred meters), other categories of models are typically simulated in a coarser resolution. As a result, they may not be suitable for capturing smoke transport or assessing the local air quality impacts from individual prescribed fires. Additionally, the lack of near-source observations makes evaluating these models' performance in prescribed burn simulations more challenging. Moreover, few studies have explored and compared CTMs and fire behavior models, which are potential tools for generating high spatiotemporal resolution smoke simulations to enhance air quality forecasting and support prescribed fire planning for fire managers. In this study, we assembled a high spatiotemporal chemical transport modeling framework, BlueSky-CMAQ, for prescribed burn simulations. The framework is a coupling of the BlueSky fire modeling framework (Larkin et al., 2009) with CMAQ to simulate the air quality impacts from prescribed fires at 1-km spatial resolution and 20-min temporal resolution. Then, we simulated

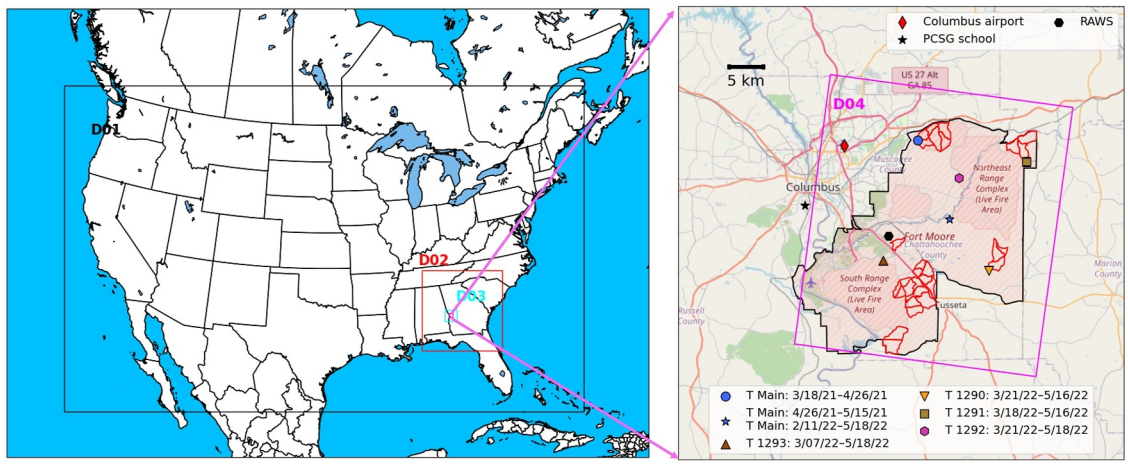

Figure 1. WRF simulation domains (left). BlueSky-CMAQ used the same domain as D03 (cyan frame), which had a 1-km resolution. WRF-SFIRE used the 200-m resolution D04 domain (pink frame), which is shown enlarged (right). The right panel also shows the boundary of Fort Benning (black line), the boundaries of studied burned units (red lines), and the locations of deployed EBAMs and trailers in the fort (dots with different colors).

prescribed burns in Fort Benning, Georgia, using BlueSky-CMAQ and WRF-SFIRE modeling frameworks. We compared the emission magnitudes, emission temporal profiles, smoke plume structures, and ground-level concentrations of pollutants between these two frameworks. Wind and $PM_{2.5}$ measurements collected in Fort Benning (El Asmar et al., 2024) were used to evaluate model performance and to understand critical factors affecting simulation performance. We expect the findings to guide future improvements and implementations of prescribed burn smoke modeling frameworks for assessing the impacts of burns on local air quality and inform fieldwork design for model evaluation.

2. Material and Methods

2.1. Study Area and Measurements

We measured $PM_{2.5}$ using a fixed site network of monitors at Fort Benning Army Base, sampling throughout the prescribed burning period during 2021 and 2022 (monitor locations are shown in Figure 1). Fort Benning, located in west central Georgia, US, typically schedules prescribed burns yearly as a land management tool to protect the ecosystem and reduce wildfire risks. In 2021, we deployed a research trailer equipped with a tapered element oscillating microbalance (TEOM) and two portable environmental beta attenuation mass monitors (EBAMs) in the fort. In the following year, we deployed more monitors, including five trailers with TEOMs and two EBAMs, to increase the probability of capturing smoke from prescribed burns in the fort and to better understand the $PM_{2.5}$ spatial distribution. The internal sampling frequency of the TEOM $PM_{2.5}$ measurements is 1 min, and data were averaged to 1 hr. The EBAMs measure hourly $PM_{2.5}$ concentrations (MOI, 2022). Besides $PM_{2.5}$, we measured surface wind speed and direction using the anemometers in EBAMs and acquired hourly wind observations from the Remote Automated Weather Station (RAWS) in Fort Benning. In 2022, anemometers were also deployed on the trailers but provided wind direction in a 16-point compass format. Since we processed $PM_{2.5}$ as hourly averages and the acquired RAWS wind observations had a 1-hr resolution, we focused on evaluating 1-hr-averaged simulated concentrations.

2.2. Prescribed Burns

The boundaries of Fort Benning burn units burned during the study period are shown with red boundaries in Figure 1 (the identifier of each burn unit is shown in Figure S1 of Supporting Information S1). Since these monitors were passively deployed, they were not always downwind from the burn units and did not capture high $PM_{2.5}$ during some burns. Since the study focused on smoke modeling, we first analyzed the source of smoke using the backward trajectory HYSPLIT when the measured $PM_{2.5}$ showed high peaks (Figures S2–S9 in Supporting Information S1). The detailed model setup and analyses can be found in the El Asmar et al. (2024). We only focused on the prescribed burns when HYSPLIT trajectories indicated that the source of measured high $PM_{2.5}$ was from the

fort. Also, the Fire Information for Resource Management System (FIRMS), which includes fire radiative power (FRP) from Terra Moderate Resolution Imaging Spectroradiometer (MODIS), Aqua MODIS, Suomi National Polar-orbiting Partnership (Suomi-NPP) Visible Infrared Imaging Radiometer Suite (VIIRS), and NOAA-20 (N20), had detected FRP from these burns. Then, eight prescribed burns were selected to be simulated in the study, including four in 2021 and four in 2022 (burn dates can be found in Table S1 of Supporting Information S1). Since the exact start times for these burns were not recorded, we used a Geostationary Operational Environmental Satellite-16 (GOES-16) product providing the FRP every 5 min, to estimate the fire start time. We defined the fire start time as the first time the FRP was reported from GOES-16 in the burn units. For April 24th and April 25th in 2022, GOES-16 did not detect any FRP in the burn units. We used an alternative method based on the HYSPLIT backward trajectory to estimate the fire start time. For these burns, we used the 1-km WRF simulations as meteorological input to HYSPLIT and started backward trajectory simulations from the downwind monitor at the time it first detected high $PM_{2.5}$. The fire start time is the time when the backward trajectories first intersected the burn units (Figures S8 and S9 in Supporting Information S1).

2.3. WRF-BlueSky-CMAQ

WRF version 4.2 (Skamarock et al., 2019) was applied to provide meteorological conditions for BlueSky version 4.5 (Larkin et al., 2009) and CMAQ version 5.3 (Byun & Schere, 2006). The 12-km resolution North American Mesoscale (NAM) (NCAR, 2015) data provided the initial and boundary conditions for WRF simulations. We utilized grid nudging and observational nudging with the NCEP ADP global surface (NCAR, 2004a) and upper air (NCAR, 2004b) observational weather data, as well as the measurements from our EBAM monitors and the RAWS in Fort Benning, to improve the modeling performance. Three nested domains, with 12, 4, and 1-km resolution (Figure 1), were used to enhance spatial resolution over Fort Benning and improve the simulation of smoke transport and its spatial impacts. Results from the meteorological simulations in the 1-km resolution domain drawn at 20-min time resolution were used for BlueSky and CMAQ simulations.

The BlueSky smoke modeling framework (Larkin et al., 2009) encapsulates different modules to estimate the fuel type, fuel load, fuel moisture, fuel consumption, emissions, time profile, and plume heights. The model runs as a pipeline, meaning the previous modules' outputs are inputs to the following module. In this study, we employed BlueSky to provide fire emissions inputs to CMAQ. We first converted the WRF simulations to Air Resources Laboratory (ARL) data format, which we then provided to BlueSky as meteorological conditions. BlueSky estimated the fuel type and fuel load by the 1-km resolution Fuel Characteristic Classification System (FCCS) (Prichard et al., 2019). Then, the fuel information and the meteorological conditions were used to estimate the fuel moisture by the National Fire Danger Rating System (NFDRS) (Deeming, 1972). Next, the CONSUME model (Ottmar et al., 1993) used the outputs from previous modules to calculate the heat and consumption from the burns, which were used for the emission and plume height estimations. We employed emission factors by Prichard et al. (2020) in BlueSky and used the Fire Emission Production Simulator (FEPS) (Anderson et al., 2004) and Briggs (1984) plume rise schemes. The BlueSky framework used an empirical time profile to distribute the total burned area and total emissions, including flaming, smoldering, and residual phases, to each hour and assumed the emission had a uniform vertical distribution between the plume bottom and the plume top.

Besides the FEPS and Briggs plume rise models incorporated in BlueSky, we also used Sofiev (Sofiev et al., 2012) and Freitas (Freitas et al., 2007) plume rise models, which are widely used in current chemical transport models. The total burned area reported by fire managers was used as input for Briggs, FEPS, and Freitas plume rise models. FRP is required to estimate plume height in Sofiev and Freitas plume rise models. We designed a "three-pass" method (Text S1 in Supporting Information S1) and applied it to FRP detections from FIRMS to calculate the FRP for each burn unit (Table S2 in Supporting Information S1). Since the satellite products we employed are all from polar-orbiting satellites, the detected FRP represents the overpass time. Assuming the FRP time profile would be the same as the burned area time profile provided by BlueSky, we used the daytime-detected FRP to generate time-varying FRP (details in Text S2 of Supporting Information S1).

CMAQ was employed to simulate the smoke transport and chemistry. We mapped the BlueSky emissions to Carbon Bound 6 (CB6) mechanisms (Pye et al., 2015) and incorporated the BlueSky time profile and plume heights to generate time-varying 3D fire emissions input for CMAQ (emission mapping method is detailed in Table S3 of Supporting Information S1). The national emission inventory (NEI) was applied for anthropogenic emissions, and the biogenic emissions were calculated online by the Biogenic Emission Inventory System,

version 4 (BEIS4), included in CMAQ. We set up nested domains for CMAQ simulations using the same domains employed in WRF, including the 12, 4, and 1-km resolution domains (boundaries of these domains are shown in Figure 1). The initial and boundary conditions for the 12-km resolution domain were obtained from daily average hemispheric CMAQ results. Prescribed burns were simulated in the 1-km resolution domain with a 20-min time resolution. Near-fire source simulations are sensitive to the timing of emission. However, CMAQ conducts a linear interpolation of emissions before using them in the numerical solution of the governing equations. For example, if fire emissions start at 4:00 UTC in the input file, they will be interpolated from zero to the first emission values between 3:40 and 4:00 UTC for a 20-min time resolution. To preserve the emission timing information from BlueSky, we utilized BlueSky emissions in CMAQ without emission temporal interpolation by revising the CMAQ code. With this revision, the start and end times of fire emissions and the emission fluxes used in CMAQ are the same as those from BlueSky.

2.4. WRF-SFIRE

We used WRF-SFIRE, which considers the interactions between fire and the atmosphere by coupling the WRF model with fuel moisture and fire spread models, to simulate the prescribed burns. Since fire spread is estimated using the Rothermel formula (Rothermel, 1972), requiring high spatial resolution data to account for fire spread across varied topography and fuel distribution, we appended a 200-m resolution domain (Figure 1) with a 20-m subgrid resolution for fire spread to simulate the burns following the three domains used in meteorological simulations with WRF. The boundary and initial conditions were provided by the 1-km resolution WRF simulations. Since some large eddies become resolvable at those scales, a 3D scale-adaptive turbulent kinetic energy scheme (Zhang et al., 2018) was conducted for the 200-m resolution domain to deal with the "gray zone" issue (Honnert et al., 2020). In WRF-SFIRE, the fuel type information was derived from a 30-m resolution LANDFIRE product (Ryan & Opperman, 2013), which classified the fuels into 13 categories based on the 13 Anderson fire behavior fuel model (Anderson, 1981). We processed the fuel data and only kept the fuel inside the burn units to avoid the fire spreading out of the unit. Since the burning records did not have the exact ignition patterns, we assumed all burns were started by strip head ignitions. Accordingly, the ignition lines were parallel to each other and perpendicular to the wind direction and drawn starting from the downwind end of the burn unit, moving upwind, creating a combination of head fires (designed ignition patterns were available at the project website (Li, 2025c). We also tuned the number of ignition lines to make the total burned area from WRF-SFIRE approximately equal to the reported burned area, as only part of the burn unit was burned. The original WRF-SFIRE limited the number of ignition lines to less than five. We expanded the constraint of ignition lines within WRF-SFIRE from 5 to 10 by revising the registry file to speed up the fire spreading process in some burns and to match the reported burned area. In WRF-SFIRE, the emission intensity and the time profile are estimated based on fuel consumption from the fire spread results. We used the inert tracer in WRF-SFIRE to simulate $PM_{2.5}$ in the smoke from prescribed burns since the measurements used in the study were mostly near-source where primary $PM_{2.5}$ is typically the main concern. To better characterize the emissions from southeastern fuels, we set the emission factors based on the southeastern US prescribed fire studies collected by the Smoke Emissions Reference Application (SERA) (Prichard et al., 2020) (Table S4 in Supporting Information S1). Unlike the BlueSky-CMAQ modeling framework using the offline plume rise schemes in WRF-SFIRE, the vertical structure of the smoke is derived from the buoyancy generated by the heat released from the fire.

3. Results

For the simulated eight prescribed burns, we compared BlueSky-CMAQ under different plume rise scheme settings with WRF-SFIRE on fuel consumptions, emission intensity and time profile, plume height, and ground-level concentrations. These models' performance was evaluated by comparing the simulated concentrations at monitor locations with measured concentrations. Here, we report statistical comparisons of all these burns simulated by different models or model settings. Detailed comparisons of simulations for each prescribed burn can be found on the project website (Li, 2025c). Additionally, we analyze how the estimated fire start time, FRP from different satellite products, and biased wind simulation affect the concentration simulations.

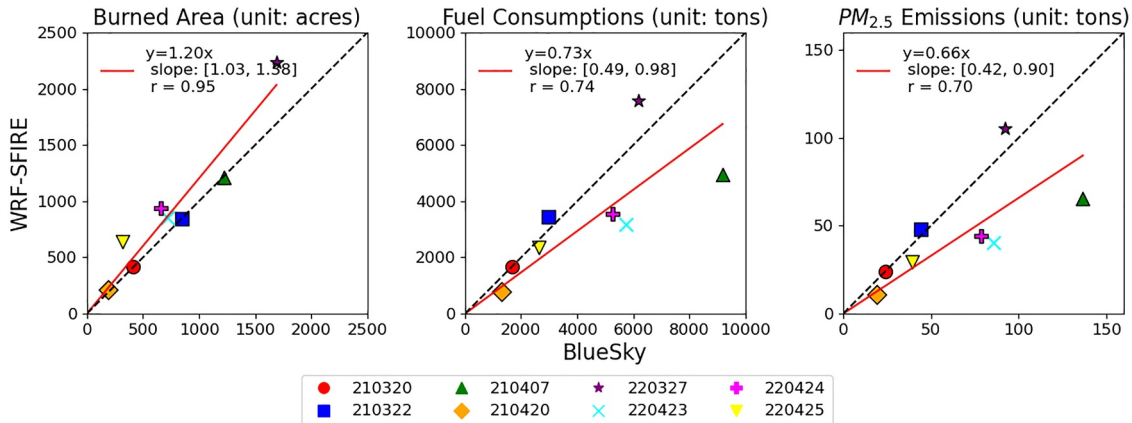

Figure 2. Comparisons between BlueSky and WRF-SFIRE estimated total burned areas (unit: acres), fuel consumptions (unit: metric tons), and $PM_{2.5}$ emissions (unit: metric tons). The zero-intercept linear regression relations between BlueSky and WRF-SFIRE, the 95% confidence intervals of slopes, and the correlations are indicated in the legend. The black dashed line is the unity (1:1) slope line, and the red line is the regression line.

3.1. Model Comparisons

3.1.1. Burned Area, Fuel Consumption, and Emissions

We directly input the reported burned area to the BlueSky framework, while in WRF-SFIRE, we bounded the burned area by removing the fuels from outside the burned units. Since the burned units were not completely burned during prescribed burn treatment and the reported burned areas are smaller than the areas of the burned units, the WRF-SFIRE burned area tended to be higher than BlueSky. Therefore, we tuned the ignition patterns in WRF-SFIRE simulations, including the number of ignition lines and the width of each ignition line, to reduce the differences between the WRF-SFIRE- and BlueSky-burned areas. We tuned the number of ignition lines by increasing or decreasing their count. We initially set the width of each ignition line as 20 m, matching the subgrid resolution of WRF-SFIRE, and increased it with an increment of 20 m. During the tuning process, we found that adjusting the number of ignition lines was more effective than changing the width of ignition lines. With tuned ignition patterns, the burned area simulated by WRF-SFIRE was 20% higher than the reported burned area used as input to BlueSky, but the correlation between them ($r = 0.95$) (Figure 2). The fuel categories are different between these two frameworks. For the simulated prescribed burns, Darlington oak forest was the most reported fuel category in BlueSky, with a burned area of 2821 acres, while in WRF-SFIRE, the most burned fuel category was brush, covering 1949 acres (Figure S10 in Supporting Information S1). For fuel consumption, we calculated the total consumption from different fuel categories for each burn. Closed short needle timber litter was the fuel with the most consumption in WRF-SFIRE, with 6,713 tons (Figure S11 in Supporting Information S1). In BlueSky, "litter-lichen-moss" was the predominant consumed fuel category, with 15,715 tons (Figure S11 in Supporting Information S1). Although the WRF-SFIRE-burned area was 20% higher than BlueSky, the fuel consumption was 27% lower than BlueSky's (Figure 2). The differences can be explained from two aspects. First, BlueSky and WRF-SFIRE used different fuel categories, resulting in variations in fuel load and, consequently, fuel consumption. The FCCS fuelbeds in BlueSky tend to have higher fuel loadings than the Anderson fuel models in WRF-SFIRE. The Anderson fuel models were designed for fire behavior needs and do not necessarily include all fuelbed components, while the FCCS provides a comprehensive description of all the fuel components for a fuelbed. Second, the models applied different consumption modules, which may lead to discrepancies in consumption intensity. WRF-SFIRE solved the Rothermel formula based on fuel and meteorological conditions, while BlueSky applied the CONSUME model, which relied on empirical formulas for different fuel types. The $PM_{2.5}$ emissions comparison between WRF-SFIRE and BlueSky showed a similar pattern to the fuel consumption comparison, with the WRF-SFIRE emissions being 34% lower than BlueSky (Figure 2). This similarity is due to both systems applying the same emission factors from SERA (Prichard et al., 2020). However, WRF-SFIRE only considered the emissions from the flaming phase because the Rothermel formula used in WRF-SFIRE is not applicable to smoldering fires (Andrews, 2018), while BlueSky estimated the emissions from both flaming and smoldering phases. For this reason, the difference of emissions between these two models is larger.

3.1.2. Plume Height

The plume schemes incorporated in the BlueSky framework assumed the emissions during the flaming phase were uniformly distributed between the plume top and the plume bottom. During the smoldering phase, emissions were injected into the surface level. WRF-SFIRE simulates the fire propagation process and estimates the heat flux emitted from the burns. The plume is elevated by the buoyancy generated from the emitted heat flux. Unlike the uniform distribution assumption used in BlueSky plume schemes, the WRF-SFIRE plume allows a variable vertical distribution driven by buoyancy. For plume height estimation in each WRF-SFIRE grid cell, we defined the height as the altitudes at which 90% of the total mass within the vertical column is contained. Then, we defined the maximum WRF-SFIRE plume height along the plume centerline for each time step (details in Text S3 in Supporting Information S1) as the plume top in WRF-SFIRE. For the simulated prescribed burns in Fort Benning, the Briggs scheme had the highest average plume top height (1,483 m), exceeding Freitas (1,324 m), WRF-SFIRE (1,319 m), FEPS (1,307 m), and Sofiev (535 m). The maximum plume top heights from WRF-SFIRE, Freitas, FEPS, and Briggs all exceeded 2700 m, significantly differing from the Sofiev plume rise scheme's maximum plume height of 897 m. We also compared the plume top heights from Briggs, FEPS, Freitas, and Sofiev to WRF-SFIRE's (Figure 3). The correlations between these offline plume schemes and WRF-SFIRE were lower. Briggs had the highest correlation with WRF-SFIRE while still lower than 0.11. However, the relative intensities of plume heights estimated by Briggs, FEPS, and Freitas were close to WRF-SFIRE's as the regression slope was close to 1. Sofiev had the lowest plume top height compared to other schemes, which was 44% of the WRF-SFIRE plume heights, as indicated by the slope. The Sofiev plume was also lower than FEPS or Briggs since the scheme considers the plume widening due to the entrainment of the surrounding air. Instead of using all the energy to uplift the smoke, the energy is partly dissipated during the smoke expansion. Additionally, the discrepancies among these plume schemes arise from variations in the definitions of plume centerlines or plume heights used during formula derivation, as well as differences in the plume height observations used to parameterize the schemes. We also analyzed discrepancies between different plume height estimations in predicting whether a plume was above or below the PBL by showing the estimates with different colors (Figure 3). The Freitas plume rise scheme showed the smallest discrepancy, with 43% of plume heights classified differently from WRF-SFIRE, while the Sofiev scheme had the largest discrepancy with 73%.

3.1.3. Ground-Level Concentration and Model Performance

We visualized the spatial distribution of simulated ground-level $PM_{2.5}$ during the prescribed burns for BlueSky-CMAQ under different plume rise schemes and WRF-SFIRE (animations showing the time evolution are available on the project website (Li, 2025c). The BlueSky-CMAQ showed a similar ground-level concentration pattern under different plume rise schemes, which indicated insensitivity to plume rise scheme. The plume shape simulated by BlueSky-CMAQ had a narrow boundary near the source and expanded during plume transport due to diffusion and entrainment, except for the simulation on 25 April 2022. The insensitivity to different plume rise schemes can be explained by the representation of fire emissions as a line source with a uniform vertical structure in the BlueSky framework. Since the BlueSky-CMAQ framework does not consider buoyancy during plume transport, when the wind direction is relatively steady, the smoke remains in a narrow band. The plume shape can be more complex when the wind direction has large spatial variability (e.g., in the simulation case on 25 April 2022). WRF-SFIRE showed a significantly different spatial concentration pattern compared to BlueSky-CMAQ. First, the plume boundary in WRF-SFIRE was narrower than BlueSky-CMAQ, in part due to the higher resolution setting in WRF-SFIRE. Also, the WRF-SFIRE plume retained energy during transport and continued to accelerate in the vertical direction due to the buoyancy, which could not be simulated in BlueSky-CMAQ. Additionally, the wind fields of WRF-SFIRE and BlueSky-CMAQ differed. CMAQ used 1-km WRF wind fields for transport while WRF-SFIRE used the same fields as initial and boundary conditions. WRF-SFIRE used a large eddy simulation for turbulence and considered the fire-atmosphere interaction when generating the wind field. Moreover, WRF-SFIRE treated the fire emissions as a 3D variable changing over time, compared to BlueSky-CMAQ that injected them in a single vertical column. Though both BlueSky-CMAQ and WRF-SFIRE used the same fire start time, WRF-SFIRE had lower emission rates at the beginning as the fire started to propagate. In contrast, BlueSky's emissions started with higher emission rates and assumed the flaming phase emissions were uniformly distributed during ignitions.

We evaluated the models by comparing simulated ground-level $PM_{2.5}$ concentrations with observations at downwind monitor sites. The hourly averaged simulated concentrations after the fire start time were calculated

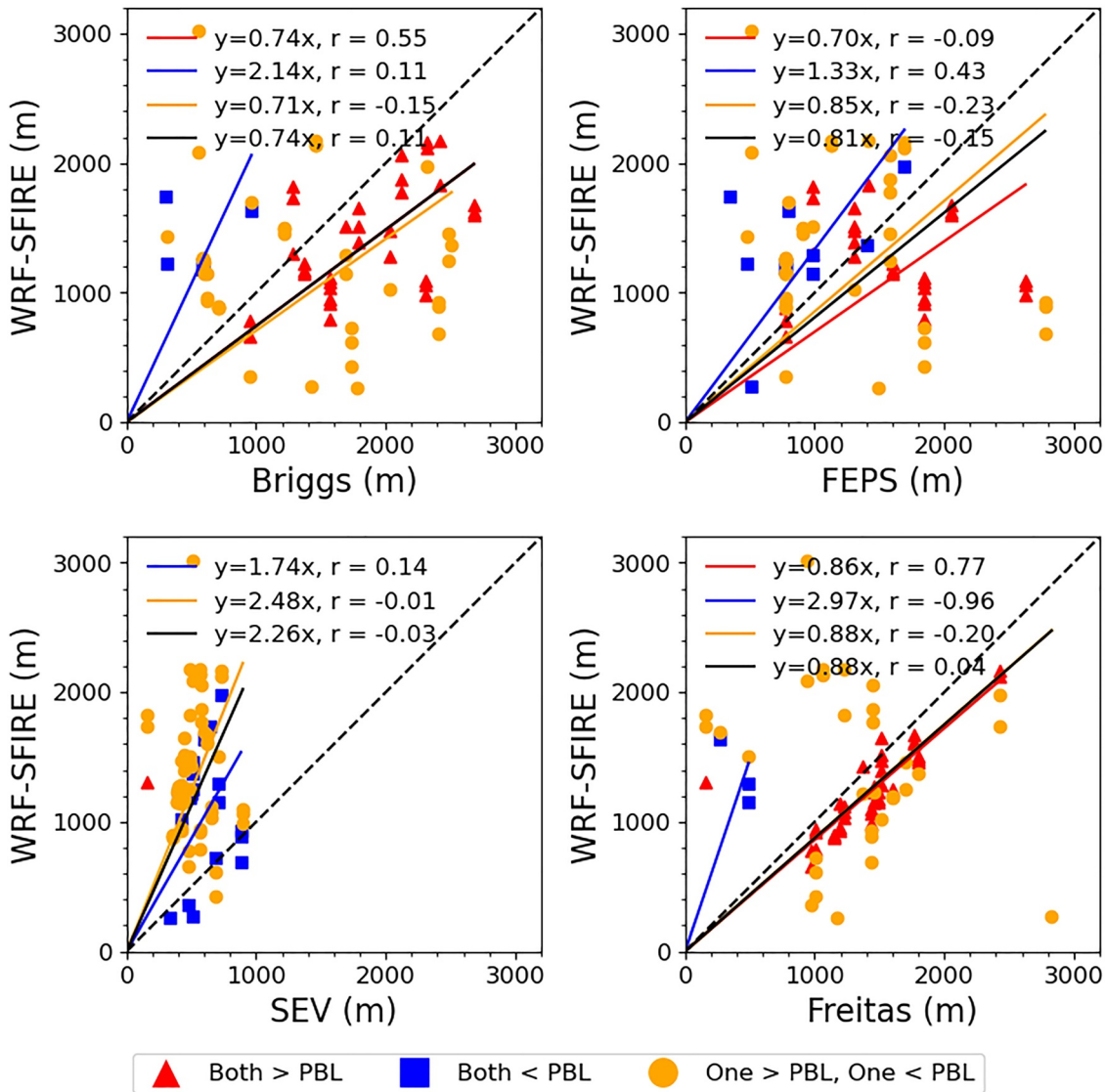

Figure 3. Comparisons between plume heights from different offline plume schemes (Briggs, FEPS, Sofiev, and Freitas) and WRF-SFIRE. Each point shows the 20-min average plume height above ground level (unit: m). The red dots indicate plume heights from both offline plume rise schemes and WRF-SFIRE exceeding the planetary boundary layer (PBL) height, while blue dots indicate both plume heights below the PBL height. The orange dots indicate cases where one plume height exceeds the PBL height while the other remains below it. The black dashed line is the unity (1:1) slope line. The red, blue, and orange lines show the linear regression for the corresponding colored dots. The black line shows the linear regressions for all the dots. The correlation r and the formula of linear regressions are indicated in the legend.

and compared with corresponding hourly averaged observations (Figure 4). Overall, WRF-SFIRE had the highest correlation with observation ($r = 0.29$), while BlueSky-CMAQ with the Freitas plume rise scheme showed the best performance for simulating the intensity of smoke (slope = 0.93). WRF-SFIRE underestimated $PM_{2.5}$ on March 20th and March 22nd in 2021 and March 27th in 2022. Although the total $PM_{2.5}$ emissions were higher in WRF-SFIRE than in BlueSky on these days (Figure 2), the narrower plume simulated by WRF-SFIRE caused the monitors to be impacted by the plume's edge, where the concentration was lower. Also, WRF-SFIRE did not simulate the background $PM_{2.5}$ and the secondary organic aerosol, which was formed in the measured smoke indicated by El Asmar et al. (2025). For understanding the secondary organic aerosol (SOA) formation during the smoke transport, we analyzed the smoke concentrations from CMAQ simulations, which are calculated by the differences between BlueSky-CMAQ simulations with and without the emissions of studied burns. At the monitoring locations, SOA can be a major portion of total $PM_{2.5}$, especially for sites far away from the burns (e.g., T-1292 on 25 April 2022; Figures S18–S21 in Supporting Information S1). However, the difference in total

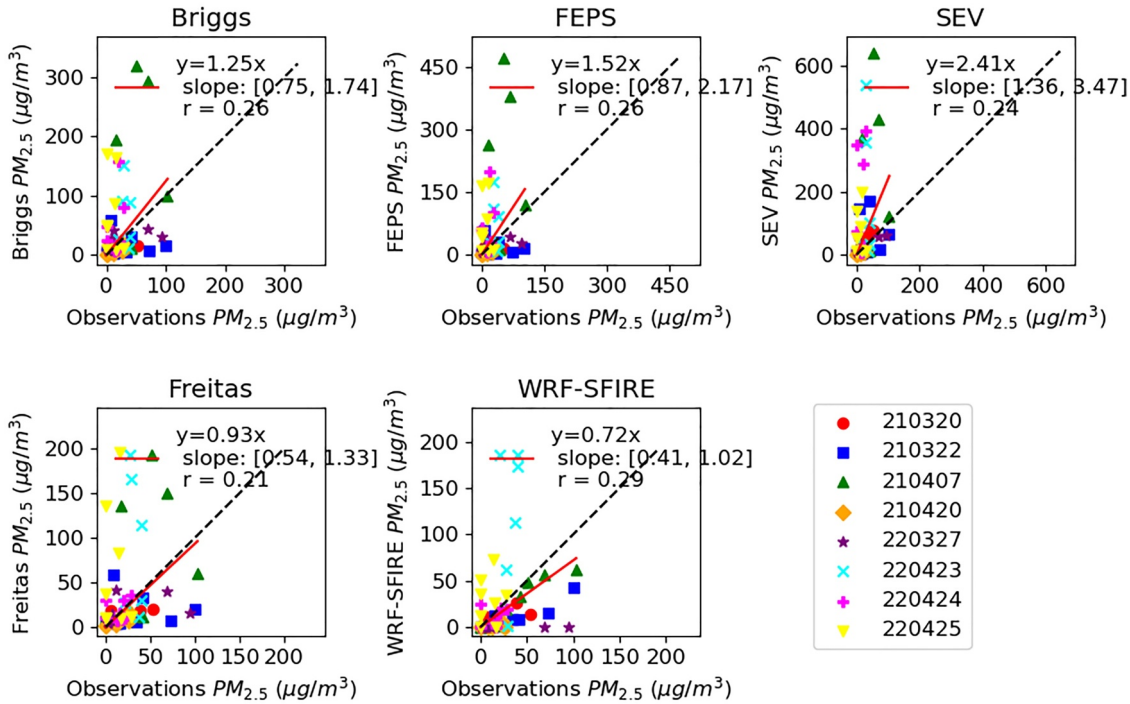

Figure 4. Comparisons between observations and simulated concentrations from BlueSky-CMAQ under different plume schemes (Briggs, FEPS, Sofiev, and Freitas) and WRF-SFIRE during the burning periods. Each scatter shows the hourly averaged ground-level $PM_{2.5}$ concentration (unit: $\mu g/m^3$). The zero-intercept linear regression relations between the compared concentrations, the 95% confidence intervals of slopes, and the correlations are indicated in the legend. The black dashed line is the unity (1:1) slope line, and the red line is the linear regression line.

$PM_{2.5}$ may not be as large when SOA formation is neglected, because primary organic $PM_{2.5}$, especially semi-volatile components, tends to decrease with plume aging (Figure S22 in Supporting Information S1). This reduction in primary mass can partially offset the additional mass contributed by SOA formation, a phenomenon also reported in a previous wildfire study (Palm et al., 2020). In BlueSky-CMAQ, the Sofiev plume rise scheme resulted in the highest smoke concentrations. Since Sofiev scheme had the lowest plume height, the emissions were concentrated at lower altitudes, which increased the ground-level concentrations. BlueSky-CMAQ performed poorly on 22 March 2021, and 7 April 2022. For the March 22nd burn, this can be explained by the unrealistic emission time profile. The simulated concentration increased sharply at the beginning of the fire since the flaming phase emission rate was assumed to be uniform during the ignition period, potentially overestimating emissions at the start of the fire. For April 7th, the BlueSky-CMAQ tended to diffuse the plume relatively quickly due to its coarse resolution, so the simulated smoke impacts had a wide range. Although no smoke was measured at the main trailer, BlueSky-CMAQ simulated more than 200 $\mu g/m^3$ at that location. All modeling frameworks had limitations on the simulation of the burns on April 23rd and April 25th in 2022. On April 23rd, the observed $PM_{2.5}$ peak timing was over 2 hr earlier than the simulations. The disparities could be explained by the significant uncertainty on fire start time since the fire start time reported by fire managers was more than 5 hours earlier than the GOES-16 detection time. On April 25th, the wind exhibited significant spatial variance, causing the main trailer, which was farther from the burn unit than T-1293, to detect the smoke earlier. However, the simulated concentrations did not reflect this pattern, possibly due to limitations in wind simulations. When we excluded these two days from the model evaluation, the performance of all the models improved, especially WRF-SFIRE, which showed a correlation of 0.66 with observations (Figure S12 in Supporting Information S1).

3.2. Uncertainty Analyses

We performed a sensitivity analysis of fire start times, FRP detections from different satellite products, and simulated wind bias to assess their impacts on smoke simulations. To investigate the impacts of fire start times, we simulated the prescribed burns on 23 April 2022, using fire start times obtained from fire managers, GOES-16, and estimates derived from HYSPLIT back trajectories (Figure S7 in Supporting Information S1). We compared

the simulated concentrations with observations at T-1293, which was 8.3 km downwind from the centroid of the burn unit. For all the simulation frameworks, using reported fire start times resulted in simulated smoke reaching the monitor earlier than observed, while using fire start times reported by GOES-16 caused the simulated smoke to reach the monitor later than observed. The timing of the smoke peak simulated by HYSPLIT back trajectories showed the best alignment with the observations (Figure 5). The smoke reached the monitor later in WRF-SFIRE than BlueSky-CMAQ since WRF-SFIRE had a lower emission rate at the beginning of the fire. Fire start times also influenced concentration intensity. For BlueSky-CMAQ, simulations using the earlier reported fire start times produced the highest concentrations due to the lower PBL heights in the morning. However, simulations using GOES-16, fire start times resulted in the highest concentrations in WRF-SFIRE. In WRF-SFIRE, higher wind speeds and lower fuel moisture in the afternoon accelerated fire propagation and increased emission rates; hence, the ground-level concentrations were higher. These meteorological conditions had less impacts on BlueSky consumption model, making PBL height the dominant factor in determining smoke concentration in BlueSky-CMAQ simulations.

Sofiev and Freitas plume rise schemes use FRP to estimate the plume heights. The satellite product that had the greatest number of FRP detections was used by applying the three-pass method. However, the FRP from different satellite products can have significant disparities (Table S2 in Supporting Information S1). The differences can be partly attributed to the varying detection times of different satellites. For instance, Terra MODIS typically reports FRP around 10:30 local time, while other satellite products detect the FRP around 13:30 local time. The FRP differences can also be found even when the satellite products had similar detection time and spatial resolution. For example, Suomi-NPP VIIRS and NOAA-20 VIIRS reported FRP for burn unit N30-C as 126.9 and 65.6 megawatts, respectively. To understand the impacts of uncertain FRPs on Sofiev and Freitas schemes, we simulated the plume height with different satellite products (Figure S13 in Supporting Information S1). For the daily average plume top, 72.2% of burn units reported less than a 20% relative difference (calculated as the difference between the maximum and minimum plume heights relative to the minimum plume height) when using different FRP inputs for the Freitas scheme, compared to only 33.3% for the Sofiev scheme. This indicates that the Freitas scheme was less sensitive to FRP variations in the simulation cases. For burn unit N30-C, the Freitas scheme showed little variation in average plume height, whereas the Sofiev scheme displayed a relative difference of 211%, with minimum and maximum plume heights of 290 and 903 m, respectively.

The prescribed burn on 25 April 2022 was the most interesting burn simulated since the smoke impacted five out of six monitors. Also, the smoke first affected the main trailer, T-1292, and USFS 1078, which were relatively far from the burn unit. Then, the smoke heavily affected T-1293 and slightly affected USFS 1079. However, no modeling frameworks captured the pattern indicated by observations due to the difficulty of simulating the complex wind field on that date. For BlueSky-CMAQ, the simulated smoke significantly affected all monitors due to the coarser resolution and poor performance on wind simulations, with $PM_{2.5}$ concentrations exceeding 100 $\mu g/m^3$. For WRF-SFIRE, the smoke concentration was highly underestimated at T-1293, USFS 1078, and T-1292. To understand the impacts of biased wind simulations on the concentration simulations, we first applied the equal time backward/forward trajectory smoke model evaluation method for the WRF-SFIRE (Li et al., 2026). The backward trajectory step aimed to find the smoke source using observed wind, and the forward trajectory step then used the simulated winds to determine where that smoke would be transported. The simulated smoke concentrations at such destination account for the impacts of wind simulation biases on the smoke concentration simulations. However, the smoke source we found was not close to the burn unit. This could partly be due to the spatial variance of the wind, which the sparse monitors did not capture. Meanwhile, the anemometers deployed on trailers reported wind direction only in a 16-point compass format, which could be off by as much as 22°. We used the equal time backward/forward trajectory method by adding a correction term for the wind observations based on prior knowledge (details of the method are in Text S4 and Figure S14 in Supporting Information S1) that the smoke source was the burn units S42-A and S42-B (Figure S1 in Supporting Information S1). The simulation results (shown in Figure 6) suggested that the main trailer and T-1293 were more likely to be affected by the smoke, while T-1290 had a lower likelihood of impact, accounting for biases in the wind simulation. However, we still found the concentration peaks had timing offset compared to observations, especially at USFS 1078, USFS 1079, and T-1293, which could be attributed to the bias on fire start time or the unrealistic ignition patterns used in WRF-SFIRE.

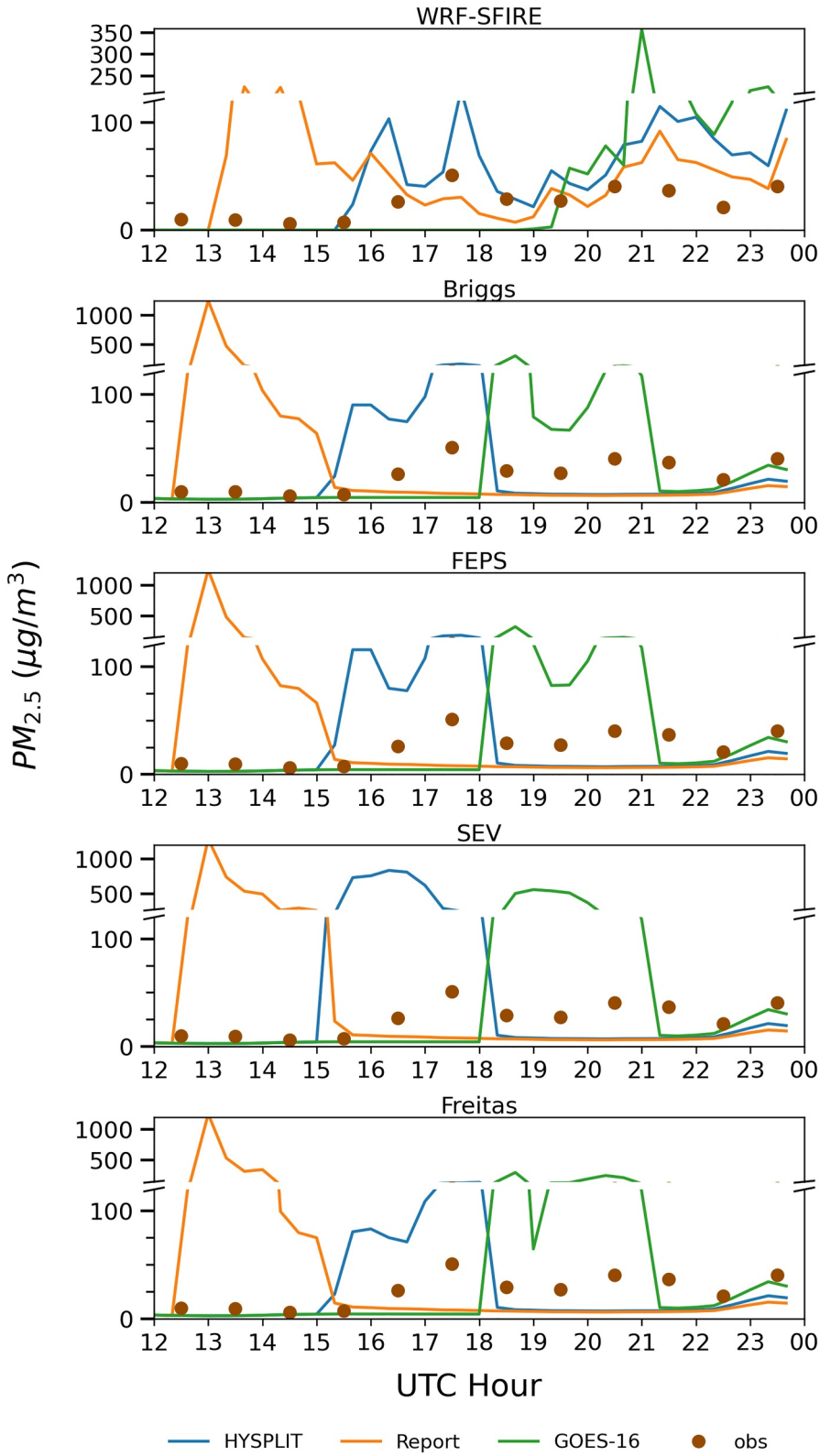

Figure 5. Observed (brown dots) and simulated (solid lines) $PM_{2.5}$ concentration (unit: $\mu g/m^3$) at T-1293 on 23 April 2022. The fire start time was estimated from three sources—HYSPLIT back trajectories (blue line), fire manager report (orange line), and GOES-16 (green line)—for each modeling framework, including WRF-SFIRE and BlueSky-CMAQ with Briggs, FEPS, Sofiev (SEV), and Freitas plume rise schemes.

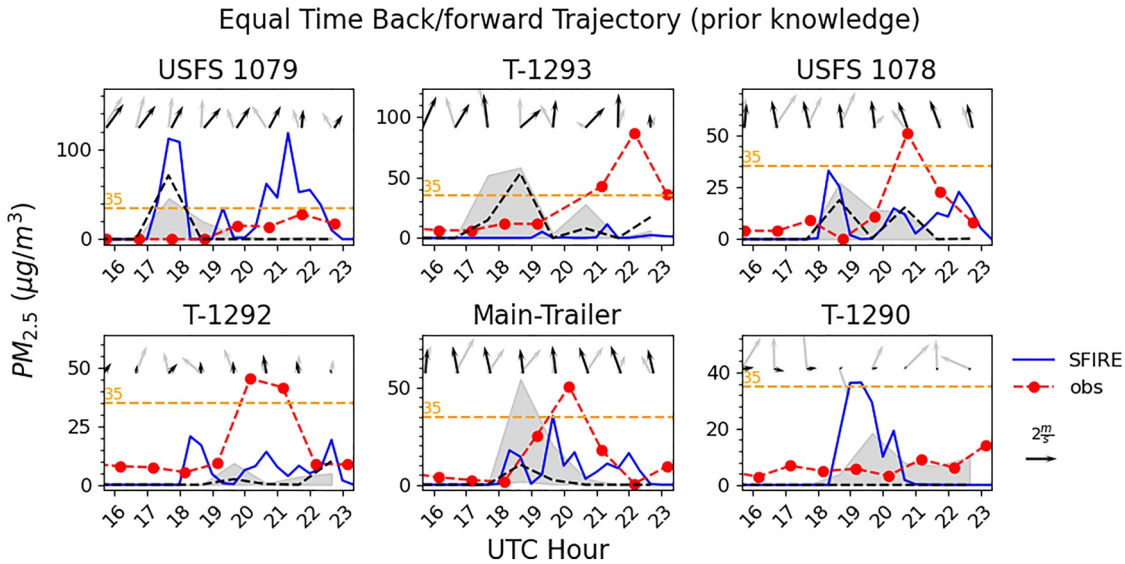

Figure 6. Observed (red dots with dashed line), WRF-SFIRE-simulated (blue solid line), and corrected $PM_{2.5}$ (black dashed line) at six monitors on 25 April 2022 by the using equal time backward/forward trajectory method with prior knowledge. The shaded area indicates the concentration uncertainty by considering the wind uncertainty along the trajectory. The black and gray arrows indicate the observed wind and modeled wind at the assigned meteorological monitor, respectively. The orange dashed line marks the 35 μg/m^3 $PM_{2.5}$ level, which is the daily standard in the U.S. (Agency, 2012).

4. Summary and Discussion

In this study, we applied BlueSky-CMAQ with different plume rise schemes and WRF-SFIRE to simulate the air quality impacts from prescribed burns in Fort Benning under high spatiotemporal resolutions. Both frameworks have advantages and disadvantages for smoke simulations. WRF-SFIRE uses a high spatial resolution LANDFIRE product to represent the heterogeneity of fuels during fire spread. On the other hand, BlueSky FCCS uses a coarser spatial resolution product but more detailed in fuel categories for a better estimation of emissions. WRF-SFIRE estimates fuel consumption based on simulated fire spread and fuel load characteristics, whereas BlueSky uses the empirical CONSUME model with a more detailed representation of different phases of fuel consumption, including flaming, smoldering, and residual. Due to the differences in fuel and consumption estimation methods, WRF-SFIRE had lower total fuel consumption and emissions than BlueSky, though it had higher burned areas. Additionally, the time profile and vertical profile of fire emissions showed disparities between different models. BlueSky assumes the flaming emissions are uniformly distributed during the fire ignition process and uses an empirical time profile to distribute smoldering and residual emissions. However, such a time profile assumption could lead to an overestimation of emissions at the beginning of the fire. Also, the vertical profile of emissions was assumed to be uniform for all these schemes. For WRF-SFIRE, the emission time profile is derived based on the fire propagation process. Due to the differences in the emission time profile, we found the smoke concentration increased quicker with a steeper gradient in CMAQ than WRF-SFIRE in the simulated cases. The choice of plume rise scheme in BlueSky-CMAQ affects the ground-level concentration intensity and spatial distribution. Sofiev and Freitas schemes use FRP to estimate plume height. However, uncertainties in satellite detection and inconsistencies between satellite products can reduce the benefits of using FRP, particularly for the Sofiev scheme, which was more sensitive to FRP inputs than the Freitas scheme. The Sofiev scheme produced higher ground-level concentrations than other plume rise schemes due to its lower plume heights. Unlike its intensity, spatial distribution of ground-level concentration was not sensitive to the choice of plume rise schemes. The concentration correlations between BlueSky-CMAQ with different plume rise schemes were high ($r > 0.86$) (Figure S15 in Supporting Information S1). For plumes rising above the PBL, ground-level concentrations were dominated by smoldering emissions injected at the surface level, with minimal influence from plume height. For plumes remaining in the PBL, fast vertical mixing in CMAQ resulted in similar smoke structures across different schemes, varying mainly in intensity. Hence, the BlueSky-CMAQ simulations with different plume rise schemes are highly correlated. WRF-SFIRE showed a low correlation ($r = 0.21$) with BlueSky-CMAQ with Briggs plume rise scheme. WRF-SFIRE uses simulated heat flux to elevate the plume. The 3D smoke structure indicates that the smoke plume continues to rise during

transport due to buoyancy as shown in the animations provided on the project website (Li, 2025c). This may decrease the ground-level concentration, a phenomenon not captured in BlueSky-CMAQ due to the simplification of plume vertical motions. Overall, WRF-SFIRE, which requires higher resolution and accounts for atmosphere-fire interactions, has greater computational complexity but offers more detailed fire behavior modeling than BlueSky-CMAQ for more realistic plume simulations.

Both frameworks reported a correlation higher than 0.2 with hourly $PM_{2.5}$ observations. WRF-SFIRE had the highest correlation with observation ($r = 0.29$), and BlueSky-CMAQ with the Freitas plume rise scheme showed the best performance for simulating the intensity of smoke measured on the ground. The comparison between observations and simulations revealed a bifurcation pattern (Figure 4): When the model-predicted smoke impacts, the monitor showed no impact or vice versa. However, this typical performance evaluation method of comparing simulated and observed concentration at the same location and hour may not be suitable for the smoke model evaluation and could underestimate the model's skill for capturing smoke. Comparisons between time series from observations and simulations (Figure S16 in Supporting Information S1) showed that both frameworks successfully simulated smoke traveling downwind to the monitor, except when the CMAQ showed no smoke impacts at T-1291 and WRF-SFIRE highly underestimated the smoke impacts at T-1292 on 27 March 2022. However, discrepancies in the timing of smoke peaks between observations and simulations reduced the model's performance. Uncertainties in fire start time and simulated wind conditions can explain the differences in smoke peak timing between simulations and observations. The fire start time would directly influence the time when the smoke reaches the downwind monitor, with an earlier fire start time resulting in an earlier peak. Similarly, an overestimated wind speed in meteorological simulations would reduce the transport time from the source to the monitor, leading to an earlier simulated smoke peak.

Challenges remain in both field measurements and smoke modeling for prescribed burns, requiring further research and development. For field measurement or data collection, the burn date, burned area, and burned location were the basic information to create the fire emission. Using the fire behavior model to simulate a typical prescribed burn additionally requires the ignition pattern, which was guesstimated based on the burn unit boundaries and wind direction in this study. However, the prescribed burn needs to be more accurately described to improve the modeling performance. Fire start time, which affects the timing of emissions, could be key information for improving the performance of both CTM and the fire behavior model and can be easily recorded. In this study, we used GOES-16 as one of the tools to estimate the fire start time, but since GOES-16 needs heat energy to reach its detection limits, the actual start time may be earlier. Additionally, cloud cover or heavy smoke can also affect satellite detections. Burned area boundaries (or firebreaks) and ignition patterns are crucial for correctly capturing the fire spread in the fire behavior model and improving the emission estimation accuracy for both frameworks. The burned areas were smaller than the areas of the burn units, but since we did not have information on which parts were burned, in WRF-SFIRE, we constrained the fire by the boundaries of the burned units. BlueSky used the centroid of the burn unit and the burned area to estimate the emissions. WRF-SFIRE requires ignition patterns to start the fire spread, and the patterns affect the burned area, emission intensity, and emission profile. Recording this information could enhance understanding of how ignition patterns affect air quality, helping to guide future prescribed burning strategies to minimize air quality impacts. Moreover, the study only measured the surface wind and ground-level concentrations during the prescribed burns. The vertical structure of smoke is an important factor affecting ground-level concentrations. For example, smoke plume height affects ground-level concentration intensity, and wind speeds and wind directions at different altitudes affect the transport of smoke. Understanding the performance of plume rise scheme or physics-based plume heights needs plume height measurements. An alternative source for plume height observations is satellite data, such as the Cloud-Aerosol Lidar and Infrared Pathfinder Satellite Observation (CALIPSO). However, CALIPSO has a narrow scanning swath (100 m footprint width) (Thomason et al., 2007) and captures data along its path only at specific times, making it prone to missing smoke from many fire sources. During the study period, CALIPSO passed over Georgia and surrounding regions only three times, and its tracks were far from Fort Benning, where the burns occurred (Figure S17 in Supporting Information S1). Another challenge is that even when CALIPSO detects plume heights, the smoke source is not explicitly identified. Identifying the source requires methods such as backward trajectory simulations (e.g., HYSPLIT), which become difficult when multiple plumes contribute to the observed plume heights. For these reasons, CALIPSO is not well suited for case studies such as those in here. For wind measurements, the sparse coverage of surface wind monitoring sites and the lack of upper-air wind observations make it challenging to understand smoke transport trajectories or accurately estimate smoke age. For

example, when we used the observed wind to drive the backward trajectory in the backward-forward trajectory smoke evaluation method to find the smoke source, the backward trajectory destination was far away from the burn unit. Compared to surface winds, transport winds at higher altitudes play a more critical role in smoke transport. However, measurements of these winds were unavailable. We found WRF-SFIRE, as a fire behavior model, performed better in providing realistic emission time or vertical profiles than BlueSky-CMAQ as a CTM. Also, WRF-SFIRE can simulate prescribed burns under different ignition pattern designs, which cannot be considered in CTMs. BlueSky-CMAQ provided detailed emission estimates by incorporating detailed fuel type classifications and accounting for emission factor variations across different fire phases. Additionally, its advanced chemical mechanisms and computational efficiency make it well suited for air quality assessments. Future work on prescribed fire modeling could focus on coupling fire behavior models with CTMs to assess both fire behavior and air quality impacts, providing valuable guidance for fire managers in making prescribed fire decisions.

This study focused on prescribed burns in Fort Benning, where 2 years of continuous in situ measurements were available. Although both BlueSky-CMAQ and WRF-SFIRE can be applied to prescribed burns in other regions, their performance may vary with different topography, meteorology, and ignition practices. Topography can influence the fire spread rate. In mountainous terrain and on steep slopes, fires spread more rapidly upslope due to preheating of fuels (Butler et al., 2007), making them more difficult to control. Such effects warrant special consideration when conducting prescribed burns in the western U.S., where rugged terrain and complex heavy fuels make fire control more challenging. WRF-SFIRE accounts for terrain-driven variations in fire spread, which are reflected in changes to the emission time profile. In contrast, BlueSky currently neglects topographic effects on the emission time profile, which may introduce potential biases. The meteorological conditions strongly affect smoke modeling performance. At coastal or near-shore locations, meteorological models tend to exhibit large biases due to limitations in representing complex land-ocean interactions (Carvalho et al., 2014). The biased wind, which affects the fire spread rate in WRF-SFIRE and smoke transport in both smoke modeling frameworks, complicates performance evaluation. For example, a previous study focused on Fort Stewart (near the Atlantic Ocean) burns showed that the WRF-SFIRE model can have poor performance due to the biased wind simulations (Li et al., 2026). The ignition pattern is another important but underevaluated factor for both model performance and air quality management. BlueSky does not currently represent ignition pattern effects on emission time profile or plume heights, whereas WRF-SFIRE does. Here, we mainly focused on using designed line ignition patterns to initialize WRF-SFIRE. WRF-SFIRE can also simulate other ignition patterns, such as point ignitions. A thorough evaluation of ignition pattern effects could inform improvements to BlueSky time profiles and help fire managers design burns that minimize air quality impacts.

Also, the study focused on prescribed burns that are very common in the southeastern U.S. Although the smoke modeling frameworks we used are generalizable to wildfires, the fire behavior and duration can be very different between prescribed fire and wildfire. Unlike prescribed burns, which typically last less than a day, wildfires can last from a few days to weeks, making it challenging to reproduce observed growth rates and spread directions. In BlueSky, daily burned area is an input parameter and a standard hourly emission profile is applied to all wildfires (Li et al., 2025; Maji et al., 2024c). For WRF-SFIRE, wildfire propagation simulation can be improved by using a satellite-informed data assimilation product (Farguell et al., 2021). A recent application of WRF-SFIRE-Chem with such assimilation shows promising smoke simulation performance (Mallia et al., 2025). Another challenge in applying these modeling frameworks to wildfire simulations is the poor performance of current meteorological models during nighttime, especially in representing PBL and wind fields (Holtslag et al., 2013; Hu et al., 2010; Miller et al., 2019; Njuki et al., 2022). These meteorological conditions strongly influenced the simulated smoke concentrations, as discussed in this study. One potential solution is to apply bias-corrected meteorological initial and boundary conditions to high-resolution smoke simulations, which has been shown to improve wind simulations (Li et al., 2026). Future studies could extend this approach to address biases in planetary boundary layer height, thereby improving smoke model performance.

Disclaimer

The findings and conclusions in this publication are those of the authors and should not be construed to represent any official U.S. government determination or policy.

Conflict of Interest

The authors declare no conflicts of interest relevant to this study.

Data Availability Statement

The observation and simulation data used in this study are available in a publicly accessible Zenodo repository (Li, 2025a). CMAQ documentation and released versions of the source code are available on the U.S. EPA modeling site (US EPA, 2019). The WRF V4.2 model code is distributed by the National Center for Atmospheric Research (NCAR, 2020). BlueSky pipeline developed by the USDA Forest Service AirFire Research Team is available at GitHub (AirFire, 2023). WRF-SFIRE is also available at GitHub (OpenWFM, 2021). The code used for the analyses in this study is available on a GitHub website (Li, 2025b). Supporting information is available. Details of simulations for each burn dates are available at the project website (Li, 2025c).

Acknowledgments
The computational support of this work was provided through the research cyberinfrastructure resources and services of the Partnership for an Advanced Computing Environment (PACE) at the Georgia Institute of Technology, Atlanta, Georgia, USA. We thank everyone who helped us with this work, especially the authorities at Fort Benning for hosting the field studies and their support in enabling our presence and field installations. This work was supported by the United States Army Corps of Engineers under Contract W912HQ-20-C-0019 to Georgia Tech Research Corporation for the Strategic Environmental Research and Development Program (SERDP) Project RC20-1047 and the US Environmental Protection Agency under Grant 84024601.

References

Afrin, S., & Garcia-Menendez, F. (2020). The influence of prescribed fire on fine particulate matter pollution in the southeastern United States. *Geophysical Research Letters*, *47*(15), e2020GL088988. https://doi.org/10.1029/2020gl088988

AirFire. (2023). BlueSky Framework rearchitected as a pipeable collection of standalone modules. *GitHub*. Retrieved from https://github.com/pnwairfire/bluesky

Agency, U. E. P. (2012). The national ambient air quality standards for particle pollution, Revised Air Quality Standards for Particle Pollution and Updates to the Air Quality Index (AQI).

Anderson, G. K., Sandberg, D. V., & Norheim, R. A. (2004). Fire Emission Production Simulator (FEPS) user's guide, version 1.0. USDA Forest Service, Pacific Northwest Research Station, Pacific Wildland Fire Sciences Laboratory, Fire and Environmental Research Applications Team and URS Corporation (p. 97). https://www.frames.gov/documents/usfs/fera/FEPS_users_guide.pdf

Anderson, H. E. (1981). *Aids to determining fuel models for estimating fire behavior*. US Department of Agriculture, Forest Service, Intermountain Forest and Range.

Andrews, P. L. (2018). *The Rothermel surface fire spread model and associated developments: A comprehensive explanation*. Gen. Tech. Rep. RMRS-GTR-371 (p. 371). US Department of Agriculture, Forest Service, Rocky Mountain Research Station. 121.

Baker, K., Woody, M., Tonnesen, G., Hutzell, W., Pye, H., Beaver, M., et al. (2016). Contribution of regional-scale fire events to ozone and PM2.5 air quality estimated by photochemical modeling approaches. *Atmospheric Environment*, *140*, 539–554. https://doi.org/10.1016/j.atmosenv.2016.06.032

Briggs, G. A. (1984). Plume rise and buoyancy effects. *Atmospheric Science and Power Production*, *327*, 366.

Burke, M., Driscoll, A., Heft-Neal, S., Xue, J., Burney, J., & Wara, M. (2021). The changing risk and burden of wildfire in the United States. *Proceedings of the National Academy of Sciences*, *118*(2), e2011048118. https://doi.org/10.1073/pnas.2011048118

Butler, B. W., Anderson, W. R., & Catchpole, E. A. (2007). Influence of slope on fire spread rate. In B. W. Butler (Ed.), *Cook, Wayne, comps. The fire environment--innovations, management, and policy; conference proceedings. 26-30 March 2007; Destin, FL. Proceedings RMRS-P-46CD* (pp. 75–82). U.S. Department of Agriculture, Forest Service, Rocky Mountain Research Station. CD-ROM. Retrieved from https://research.fs.usda.gov/treesearch/28552

Byun, D., & Schere, K. L. (2006). Review of the governing equations, computational algorithms, and other components of the Models-3 Community Multiscale Air Quality (CMAQ) modeling system. *Applied Mechanics Reviews*, *59*(2), 51–77. https://doi.org/10.1115/1.2128636

Carter, T. S., Heald, C. L., & Selin, N. E. (2023). Large mitigation potential of smoke PM2.5 in the US from human-ignited fires. *Environmental Research Letters*, *18*(1), 014002. https://doi.org/10.1088/1748-9326/aca91f

Carvalho, D., Rocha, A., Gómez-Gesteira, M., & Silva Santos, C. (2014). Sensitivity of the WRF model wind simulation and wind energy production estimates to planetary boundary layer parameterizations for onshore and offshore areas in the Iberian Peninsula. *Applied Energy*, *135*, 234–246. https://doi.org/10.1016/j.apenergy.2014.08.082

Childs, M. L., Li, J., Wen, J., Heft-Neal, S., Driscoll, A., Wang, S., et al. (2022). Daily local-level estimates of ambient wildfire smoke PM2.5 for the contiguous US. *Environmental Science & Technology*, *56*(19), 13607–13621. https://doi.org/10.1021/acs.est.2c02934

Deeming, J. E. (1972). National fire-danger rating system, Rocky Mountain Forest and Range Experiment Station. *Forest Service, US*.

El Asmar, R., Li, Z., Tanner, D. J., Hu, Y., O'Neill, S., Huey, L. G., et al. (2024). A multi-site passive approach to studying the emissions and evolution of smoke from prescribed fires. *Atmospheric Chemistry and Physics*, *24*(22), 12749–12773. https://doi.org/10.5194/acp-24-12749-2024

El Asmar, R., Li, Z., Yu, H., O'Neill, S., Tanner, D. J., Huey, L. G., et al. (2025). Formation of ozone and PM2.5 in smoke from prescribed burning in the Southeastern United States. *ACS ES&T Air*, *2*(3), 343–357. https://doi.org/10.1021/acsestair.4c00231

Farguell, A., Mandel, J., Haley, J., Mallia, D. V., Kochanski, A., & Hilburn, K. (2021). Machine learning estimation of fire arrival time from level-2 active fires satellite data. *Remote Sensing*, *13*(11), 2203. https://doi.org/10.3390/rs13112203

Francos, M., & Úbeda, X. (2021). Prescribed fire management. *Current Opinion in Environmental Science & Health*, *21*, 100250. https://doi.org/10.1016/j.coesh.2021.100250

Freitas, S. R., Longo, K. M., Chatfield, R., Latham, D., Silva Dias, M. A. F. d., Andreae, M., et al. (2007). Including the sub-grid scale plume rise of vegetation fires in low resolution atmospheric transport models. *Atmospheric Chemistry and Physics*, *7*(13), 3385–3398. https://doi.org/10.5194/acp-7-3385-2007

Holtslag, A. A. M., Svensson, G., Baas, P., Basu, S., Beare, B., Beljaars, A. C. M., et al. (2013). Stable atmospheric boundary layers and diurnal cycles: Challenges for weather and climate models. *Bulletin of the American Meteorological Society*, *94*(11), 1691–1706. https://doi.org/10.1175/BAMS-D-11-00187.1

Honnert, R., Efstathiou, G. A., Beare, R. J., Ito, J., Lock, A., Neggers, R., et al. (2020). The atmospheric boundary layer and the "gray zone" of turbulence: A critical review. *Journal of Geophysical Research: Atmospheres*, *125*(13), e2019JD030317. https://doi.org/10.1029/2019jd030317

Hu, X.-M., Nielsen-Gammon, J. W., & Zhang, F. (2010). Evaluation of three planetary boundary layer schemes in the WRF model. *Journal of Applied Meteorology and Climatology*, *49*(9), 1831–1844. https://doi.org/10.1175/2010JAMC2432.1

Huang, R., Hu, Y., Russell, A. G., Mulholland, J. A., & Odman, M. T. (2019). The impacts of prescribed fire on PM2. 5 air quality and human health: Application to asthma-related emergency room visits in Georgia, USA. *International Journal of Environmental Research and Public Health*, *16*(13), 2312. https://doi.org/10.3390/ijerph16132312

Hunter, M. E., & Robles, M. D. (2020). Tamm review: The effects of prescribed fire on wildfire regimes and impacts: A framework for comparison. *Forest Ecology and Management*, *475*, 118435. https://doi.org/10.1016/j.foreco.2020.118435

Jaffe, D. A., O'Neill, S. M., Larkin, N. K., Holder, A. L., Peterson, D. L., Halofsky, J. E., & Rappold, A. G. (2020). Wildfire and prescribed burning impacts on air quality in the United States. *Journal of the Air & Waste Management Association*, *70*(6), 583–615. https://doi.org/10.1080/10962247.2020.1749731

Johnson, M. M., & Garcia-Menendez, F. (2023). A comparison of smoke modelling tools used to mitigate air quality impacts from prescribed burning. *International Journal of Wildland Fire*, *32*(7), 1162–1173. https://doi.org/10.1071/wf22172

Kochanski, A. K., Beezley, J. D., Mandel, J., & Kim, M. (2012). WRF fire simulation coupled with a fuel moisture model and smoke transport by WRF-Chem. arXiv preprint arXiv:1208.1059.

Kochanski, A. K., Jenkins, M. A., Mandel, J., Beezley, J. D., Clements, C. B., & Krueger, S. (2013). Evaluation of WRF-SFIRE performance with field observations from the FireFlux experiment. *Geoscientific Model Development*, *6*(4), 1109–1126. https://doi.org/10.5194/gmd-6-1109-2013

Larkin, N. K., O'Neill, S. M., Solomon, R., Raffuse, S., Strand, T., Sullivan, D. C., et al. (2009). The BlueSky smoke modeling framework. *International Journal of Wildland Fire*, *18*(8), 906–920. https://doi.org/10.1071/wf07086

Lavdas, L. G. (1986). *An atmospheric dispersion index for prescribed burning*. US Department of Agriculture, Forest Service, Southeastern Forest Experiment.

Lavdas, L. G. (1996). Program VSMOKE-users manual, Southern Research Station.

Lee, H., & Jaffe, D. A. (2024). Wildfire impacts on O3 in the Continental United States using PM2.5 and a generalized additive model (2018–2023). *Environmental Science & Technology*, *58*(33), 14764–14774. https://doi.org/10.1021/acs.est.4c05870

Li, Z. (2025a). Comparisons of high-spatiotemporal resolution air quality modeling frameworks for prescribed burning simulations at a military base in the Southeastern United States. *Zenodo*. https://doi.org/10.5281/zenodo.17114899

Li, Z. (2025b). Analysis code for comparisons of high-spatiotemporal resolution air quality modeling frameworks for prescribed burning simulations at a military base in the Southeastern United States. *GitHub*. Retrieved from https://github.com/zli867/SERDPSmokeModelComparison

Li, Z. (2025c). Project website for comparisons of high-spatiotemporal resolution air quality modeling frameworks for prescribed burning simulations at a military base in the Southeastern United States. *GitHub*. Retrieved from https://zli867.github.io/projects/FtRxSimulation/WebSrc/index.html

Li, Z., O'Neill, S. M., Asmar, R. E., Hu, Y., Kochanski, A. K., Farguell, A., et al. (2026). An investigation of corrective approaches for uncertain winds and analysis of impacts on smoke model performance. *Agricultural and Forest Meteorology*, *376*, 110885. https://doi.org/10.1016/j.agrformet.2025.110885

Li, Z., Vaidyanathan, A., Maji, K. J., Hu, Y., O'Neill, S. M., Russell, A. G., & Odman, M. T. (2025). The trade-offs between wildfires and prescribed fires: A case study for 2016 gatlinburg wildfires. *ACS ES&T Air*, *2*, 236–248. https://doi.org/10.1021/acsestair.4c00233

Maji, K. J., Ford, B., Li, Z., Hu, Y., Hu, L., Langer, C. E., et al. (2024c). Impact of the 2022 New Mexico, US wildfires on air quality and health. *Science of the Total Environment*, *946*, 174197. https://doi.org/10.1016/j.scitotenv.2024.174197

Maji, K. J., Li, Z., Hu, Y., Vaidyanathan, A., Stowell, J. D., Milando, C., et al. (2024a). Prescribed burn related increases of population exposure to PM2.5 and O3 pollution in the southeastern US over 2013–2020. *Environment International*, *193*, 109101. https://doi.org/10.1016/j.envint.2024.109101

Maji, K. J., Li, Z., Vaidyanathan, A., Hu, Y., Stowell, J. D., Milando, C., et al. (2024b). Estimated impacts of prescribed fires on air quality and premature deaths in Georgia and surrounding areas in the US, 2015–2020. *Environmental Science & Technology*, *58*(28), 12343–12355. https://doi.org/10.1021/acs.est.4c00890

Mallia, D. V., Kochanski, A. K., Urbanski, S. P., Mandel, J., Farguell, A., & Krueger, S. K. (2020). Incorporating a canopy parameterization within a coupled fire-atmosphere model to improve a smoke simulation for a prescribed burn. *Atmosphere*, *11*(8), 832. https://doi.org/10.3390/atmos11080832

Mallia, D. V., White, C., Farguell, A., Mandel, J., & Kochanski, A. K. (2025). Simulating the impacts of regional wildfire smoke on ozone using a coupled fire-atmosphere-chemistry model. *Atmospheric Environment*, *360*, 121404. https://doi.org/10.1016/j.atmosenv.2025.121404

Mandel, J., Amram, S., Beezley, J., Kelman, G., Kochanski, A., Kondratenko, V., et al. (2014). Recent advances and applications of WRF–SFIRE. *Natural Hazards and Earth System Sciences*, *14*(10), 2829–2845. https://doi.org/10.5194/nhess-14-2829-2014

Marlon, J. R., Bartlein, P. J., Gavin, D. G., Long, C. J., Anderson, R. S., Briles, C. E., et al. (2012). Long-term perspective on wildfires in the western USA. *Proceedings of the National Academy of Sciences*, *109*(9), E535–E543. https://doi.org/10.1073/pnas.1112839109

Miller, C., O'Neill, S., Rorig, M., & Alvarado, E. (2019). Air-quality challenges of prescribed fire in the complex terrain and wildland urban interface surrounding Bend, Oregon. *Atmosphere*, *10*(9), 515. https://doi.org/10.3390/atmos10090515

Mobley, H. E. (1976). Southern forestry smoke management guidebook (Gen. Tech. Rep. SE-10, p. 140). US Department of Agriculture, Forest Service, Southeastern Forest Experiment Station.

MOI (2022). *E-BAM 9800 Manual (Rev. P)*. Met One Instruments.

NCAR. (2004a). NCEP ADP global surface observational weather data, October 1999 - Continuing [Dataset]. *Research Data Archive at the National Center for Atmospheric Research, Computational and Information Systems Laboratory*. https://doi.org/10.5065/4F4P-E398

NCAR. (2004b). NCEP ADP global upper air observational weather data, October 1999 - Continuing [Dataset]. *Research Data Archive at the National Center for Atmospheric Research, Computational and Information Systems Laboratory*. https://doi.org/10.5065/39C5-Z211

NCAR. (2015). NCEP North American Mesoscale (NAM) 12 km analysis, research data archive at the National Center for Atmospheric research, computational and information systems laboratory [Dataset]. https://doi.org/10.5065/G4RC-1N91

NCAR. (2020). The official repository for the Weather Research and Forecasting (WRF) model. *GitHub*. Retrieved from https://github.com/wrf-model/WRF

Njuki, S. M., Mannaerts, C. M., & Su, Z. (2022). Influence of Planetary Boundary Layer (PBL) parameterizations in the weather research and forecasting (WRF) model on the retrieval of surface meteorological variables over the Kenyan highlands. *Atmosphere*, *13*(2), 169. https://doi.org/10.3390/atmos13020169

OpenWFM. (2021). A coupled weather-fire forecasting model built on top of Weather Research and Forecasting (WRF). *GitHub*. Retrieved from https://github.com/openwfm/WRF-SFIRE

Ottmar, R. D., Burns, M. F., Hall, J. N., & Hanson, A. D. (1993). *CONSUME: Users guide, Gen. Tech. Rep. PNW-GTR-304* (Vol. 304). US Department of Agriculture, Forest Service, Pacific Northwest Research Station.

Palm, B. B., Peng, Q., Fredrickson, C. D., Lee, B. H., Garofalo, L. A., Pothier, M. A., et al. (2020). Quantification of organic aerosol and brown carbon evolution in fresh wildfire plumes. *Proceedings of the National Academy of Sciences*, *117*(47), 29469–29477. https://doi.org/10.1073/pnas.2012218117

Policelli, N., Picca, P., & Gómez Villafañe, I. E. (2019). Is prescribed fire a suitable management tool to reduce shrub encroachment in palm savannas? *Restoration Ecology*, *27*(1), 109–119. https://doi.org/10.1111/rec.12824

Prichard, S. J., Andreu, A., Ottmar, R. D., & Eberhardt, E. (2019). *Fuel Characteristic Classification System (FCCS) field sampling and fuelbed development guide*. US Department of Agriculture, Forest Service, Pacific Northwest Research.

Prichard, S. J., O'Neill, S. M., Eagle, P., Andreu, A. G., Drye, B., Dubowy, J., et al. (2020). Wildland fire emission factors in North America: Synthesis of existing data, measurement needs and management applications. *International Journal of Wildland Fire*, *29*(2), 132–147. https://doi.org/10.1071/wf19066

Pye, H. O., Luecken, D. J., Xu, L., Boyd, C. M., Ng, N. L., Baker, K. R., et al. (2015). Modeling the current and future roles of particulate organic nitrates in the southeastern United States. *Environmental Science & Technology*, *49*(24), 14195–14203. https://doi.org/10.1021/acs.est.5b03738

Qiu, M., Kelp, M., Heft-Neal, S., Jin, X., Gould, C. F., Tong, D. Q., & Burke, M. (2024). Evaluating chemical transport and machine learning models for wildfire smoke PM2.5: Implications for assessment of health impacts. *Environmental Science & Technology*, *58*(52), 22880–22893. https://doi.org/10.1021/acs.est.4c05922

Raffuse, S., O'Neill, S., & Schmidt, R. (2024). A model for rapid PM2.5 exposure estimates in wildfire conditions using routinely available data: Rapidfire v0.1.3. *Geoscientific Model Development*, *17*(1), 381–397. https://doi.org/10.5194/gmd-17-381-2024

Rothermel, R. C. (1972). A mathematical model for predicting fire spread in wildland fuels, Intermountain Forest & Range Experiment Station, Forest Service, US.

Ryan, K. C., & Opperman, T. S. (2013). LANDFIRE – A national vegetation/fuels data base for use in fuels treatment, restoration, and suppression planning. *Forest Ecology and Management*, *294*, 208–216. https://doi.org/10.1016/j.foreco.2012.11.003

Skamarock, W. C., Klemp, J. B., Dudhia, J., Gill, D. O., Liu, Z., Berner, J., et al. (2019). A description of the advanced research WRF version 4. *NCAR tech. note ncar/tn-556+ str*, *145*.

Sofiev, M., Ermakova, T., & Vankevich, R. (2012). Evaluation of the smoke-injection height from wild-land fires using remote-sensing data. *Atmospheric Chemistry and Physics*, *12*(4), 1995–2006. https://doi.org/10.5194/acp-12-1995-2012

Stein, A., Draxler, R. R., Rolph, G. D., Stunder, B. J., Cohen, M. D., & Ngan, F. (2015). NOAA's HYSPLIT atmospheric transport and dispersion modeling system. *Bulletin of the American Meteorological Society*, *96*(12), 2059–2077. https://doi.org/10.1175/bams-d-14-00110.1

Thomason, L. W., Pitts, M. C., & Winker, D. M. (2007). CALIPSO observations of stratospheric aerosols: A preliminary assessment. *Atmospheric Chemistry and Physics*, *7*(20), 5283–5290. https://doi.org/10.5194/acp-7-5283-2007

US EPA. (2019). Code for U.S. EPA's Community Multiscale Air Quality Model (CMAQ) for estimating ozone, particulates, toxics, and deposition of acids and nutrients at neighborhood to global scales. *GitHub*. Retrieved from https://github.com/USEPA/CMAQ

Westerling, A. L., Hidalgo, H. G., Cayan, D. R., & Swetnam, T. W. (2006). Warming and earlier spring increase western US forest wildfire activity. *Science*, *313*(5789), 940–943. https://doi.org/10.1126/science.1128834

Wilkins, J. L., Pouliot, G., Foley, K., Appel, W., & Pierce, T. (2018). The impact of US wildland fires on ozone and particulate matter: A comparison of measurements and CMAQ model predictions from 2008 to 2012. *International Journal of Wildland Fire*, *27*(10), 684–698. https://doi.org/10.1071/wf18053

Zhang, X., Bao, J.-W., Chen, B., & Grell, E. D. (2018). A three-dimensional scale-adaptive turbulent kinetic energy scheme in the WRF-ARW model. *Monthly Weather Review*, *146*(7), 2023–2045. https://doi.org/10.1175/mwr-d-17-0356.1